2020

Creating thin magnetic layers at the surface of Sb2Te3 topological insulators using a low-energy chromium ion beam

David L. Cortie
University of Wollongong, dcortie@uow.edu.au

Weiyao Zhao
University of Wollongong, wz929@uowmail.edu.au

Zengji Yue
University of Wollongong, zengji@uow.edu.au

Zhi Li
University of Wollongong, zhili@uow.edu.au

Abuduliken Bake
University of Wollongong, ab913@uowmail.edu.au

See next page for additional authors

Creating thin magnetic layers at the surface of Sb2Te3 topological insulators using a low-energy chromium ion beam

Abstract

The surfaces of Sb_2Te_3 topological insulator crystals were implanted using a 40 keV chromium ion beam. To facilitate uniform doping, the Sb_2Te_3 was passivated with a thin TiO_2 film before the implantation step. The resulting chemical structure was studied using atomic-resolution transmission electron microscopy. A fluence of 7×10^{15} ions/cm^2 at 40 keV lead to amorphization of the Sb_2Te_3 surface, with chromium predominantly incorporated in the amorphous layer. Heating to 200 °C caused the amorphous region to recrystallize and led to the formation of a thin chromium-rich interfacial layer. Near-edge x-ray absorption spectroscopy indicates a uniform valence state of Cr^{3+} throughout, with no evidence of metallic clustering. High-temperature superparamagnetic behavior was detected up to 300 K, with an increased magnetic moment below 50 K.

Disciplines

Engineering | Physical Sciences and Mathematics

Publication Details

Cortie, D, Zhao, W, Yue, Z, Li, Z, Bake, A, Marenych, O, Pastuovic, Z, Nancarrow, M, Zhang, Z, Qi, D-C, Evans, P, Mitchell, DRG & Wang, X 2020, 'Creating thin magnetic layers at the surface of Sb2Te3 topological insulators using a low-energy chromium ion beam', Applied physics letters, vol. 116, no. 19, p. 192410.

Authors

David L. Cortie, Weiyao Zhao, Zengji Yue, Zhi Li, Abuduliken Bake, Olexandra Marenych, Zeljko Pastuovic, MItchell John Bromley Nancarrow, Zhaoming Zhang, Dong-Chen Qi, Peter Evans, D RG Mitchell, and Xiaolin Wang

Creating thin magnetic layers at the surface of Sb_2Te_3 topological insulators using a low-energy chromium ion beam

David Cortie,[1,2*] Weiyao Zhao,[1,2] Zengji Yue,[1,2] Zhi Li,[1,2], Abuduliken Bake[1], Olexandra Marenych,[3] Zeljko Pastuovic,[4] Mitchell Nancarrow,[3] Zhaoming Zhang,[4] Dong-Chen Qi,[5] Peter Evans,[4] David R. G. Mitchell,[3*] Xiaolin Wang[1,2]

AFFILIATIONS

[1]*The Institute for Superconducting and Electronic Materials, The University of Wollongong, NSW 2500 Australia*

[2]*ARC Centre of Excellence in Future Low-Energy Electronics Technologies FLEET, University of Wollongong, NSW 2500, Australia*

[3]*Electron Microscopy Centre, The University of Wollongong, NSW 2500 Australia*

[4]*Australian Nuclear Science and Technology Organization, Lucas Heights, NSW 2234, Australia*

[5]*ARC Centre of Excellence in Future Low-Energy Electronics Technologies FLEET, School of Chemistry, Physics and Mechanical Engineering, Queensland University of Technology, Brisbane, Queensland 4001, Australia*

Corresponding authors: dcortie@uow.edu.au;

ABSTRACT

The surfaces of Sb_2Te_3 topological insulator crystals were implanted using a 40 keV chromium ion beam. To facilitate a uniform doping, the Sb_2Te_3 was passivated with a thin TiO_2 film before the implantation step. The resulting chemical structure was studied using atomic-resolution transmission electron microscopy. A fluence of 7×10^{15} ions/cm^2 at 40 keV lead to amorphisation of the Sb_2Te_3 surface, with chromium predominantly incorporated in the amorphous layer. Heating to 200 °C caused the amorphous region to recrystallize and led to the formation of a thin chromium-rich interfacial layer. Near-edge X-ray absorption spectroscopy indicates a uniform valence state of Cr^{3+} throughout, with no evidence of metallic clustering. High-temperature superparamagnetic behavior was detected up to 300 K, with an increased magnetic moment below 50 K.

In the past decade, elegant methods emerged to classify electronic band structures using a scheme based on topological invariants. One outcome was the discovery of the topological insulator which is an unusual type of solid that is characterized by having a bulk band-gap in conjunction with gapless metallic states at the surface[1]. In three-dimensional topological insulators (TIs) such as Sb_2Te_3, the surface states (SS) act as the domain boundary between the topological and non-topological electronic phases in the crystal and vacuum respectively[1]. Similar states also exist at the interface of a TI with ordinary "topologically-trivial" insulators (e.g. TiO_2)[2]. These gapless states offer unique properties[3,4] featuring a Dirac-like dispersion, as found in graphene, together with an exotic helical spin-texture that offers protection against a variety of electron scattering mechanisms. This presents an attractive avenue for

electronics that minimize wasteful heat dissipation[3,4]. Numerous experiments using angle-resolved photoemission spectroscopy have observed these Dirac states in vacuum[5], however, they remain challenging to isolate in real-world transport devices because of issues with band-bending, passivation and bulk leakage currents. To address these problems, doping methods have been intensively explored to modulate the Fermi level[6], to allow for defect compensation[7], to achieve p/n junctions[8], and to enable magnetic[9] and superconducting surfaces[10]. Although there has been steady progress, the standard chemical methods are complex and do not allow for accurate spatial placement of the dopant, which is an important prerequisite for scalable circuitry. For accurate lateral and vertical dopant placement, industrial work on semiconductor surfaces has relied on ion beam implantation since the 1970s[11]. However, there are very few studies of implantation in topological insulators. To achieve ideal chemical doping, it is generally desirable to remove residual defects introduced by the implantation process using a post-implantation heat treatment. In some cases, however, the ion implantation process can be used to generate desirable, functional defects (e.g. the nitrogen vacancies in diamond) to perform defect-engineering with a high level of spatial precision[12]. Recently, a theoretical work proposed that ion beams provide some additional opportunities to engineer topological transport by introducing a disordered layer of depth (d) near the surface that acts to trap the surface states, reposition the SS spatially, and enhance the in-gap density of states to produce control points ideal for gating[13]. This concept relies on tuning the disorder field to a high value to approach a quantum critical point.

To date, however, there is very little direct experimental information about the nature of disorder caused by ion beams in the delicate van der Waals (vdW) TI structures, and only a handful of articles are available as summarized below. Earlier work by Zhang et al. reported that it was advantageous to use a SiO_2 buffer layer to protect Sb_2Te_3 films before implantation with silicon ions at 50 keV to improve phase-change memory properties[14]. Later, Sharma et al. demonstrated p-type doping of Bi_2Se_3 using calcium ions at 200 keV into single crystals buffered with a 100 nm thick layer of Al_2O_3 and reported that no amorphous layer was formed at fluences of up to $1x10^{17}$ ions per cm^2[15]. β-NMR studies using Li-ion beams implanted into the bare surfaces of Bi_xSb_{1-x}[16], Bi_2Se_3 and Bi_2TeSe[17] chalcogenides showed that Li+ can be implanted at keV energies within tens of nanometres of the surface and the smaller ion intercalates into the vdW gap where it undergoes diffusion at room temperature. Leedahl et al. reported that implanting transition metals (Fe, Cr, Mn, Ni) at a moderate fluence ($1x10^{17}$ ions per cm^2) at 30 keV into bare Bi_2Te_3 surfaces leads to stable substitutional doping in the majority of cases[18]. So far, however, there has been no demonstration of transition-metal implantation at shallow depths in the near-surface region (0 – 40 nm) of Sb_2Te_3 topological insulators, which is a prerequisite for surface-state engineering. One attractive

species for this purpose is chromium (Cr) since doping is known to lead to the onset of a magnetic order that introduces a gap in the topological surface states and potentially allows for the (quantum) anomalous Hall effect[9]. In thin films grown by molecular beam epitaxy (MBE), it is possible to achieve high Cr(V) doping concentrations in Cr_x $(Sb,Bi)_2$-xTe_3 with $0.1 < x < 0.35$ having atomic percentages > 10%. However, in conventional single crystal growth, it is difficult to achieve uniform substitution above x=0.05[19], and consequently, the Curie temperature is very low ($5 < T_C < 20$ K) because T_c scales linearly with x[20]. To investigate the possibilities offered by Cr-implantation, we therefore conducted experiments on Sb_2Te_3 single crystals.

The central finding of this work is that implantation at high Cr fluences is possible in the Sb_2Te_3 crystals provided the crystals are coated with an oxide layer. As in the previous work[2,15], this acts to reinforce the surface against flaking and absorbs a large fraction of the ion beam induced damage. Figure 1a-c) summarizes the steps used in the three-step synthesis procedure. Firstly, the Sb_2Te_3 crystals were grown using a melt-based method, as previously described in Ref[21], and cleaved to reveal large-diameter (001)-orientated surfaces of ~ 5x5 mm^2 in area. Crystals were ultra-sonicated in isopropanol to remove residual dust. $TiO_{2-\delta}$ films (10 nm) were deposited using a viscous flow atomic layer deposition (ALD) reactor (ASM Microchemistry F-120) at 393 K to provide conformal amorphous thin films by exposing the crystals to sequential pulses of $TiCl_4$ (0.4 s) and H_2O (1.0 s) in N_2 carrier gas. Selected crystals were subsequently implanted with Cr ions using an ion implanter equipped with a metal vapour vacuum arc (MEVVA) ion source.[22] A 40 keV ion beam was used, and the applied implantation fluence was 7×10^{15} ions per cm^2. To prepare the cross-sections for TEM, a HELIOS Nanolab G3 instrument was used, by applying protective carbon coating and followed by focused-ion beam treatment using a 30 keV Ga beam. Figure 1d) shows a scanning transmission electron microscopy (STEM) image of the cross-section of TiO_2-coated Sb_2Te_3 crystal implanted with a fluence of 7 $x10^{15}$ Cr ions per cm^2. This is taken in high angle annular dark field imaging mode (HAADF) such that the intensity originates from the atomic-number (approximately proportional to Z^2), and consequently the low-Z titania appears as a dark region and the Sb_2Te_3 as light. Monte Carlo calculations using Stopping Range of Ions In Matter (SRIM) code[23] (Figure 1 e) indicates that the average penetration depth of the Cr-ion is 30 nm, such that the majority of Cr are transmitted through the TiO_2 layer. Energy-dispersive X-ray spectroscopy (EDS) was conducted in the STEM (Figure 1 f) and confirms a chromium profile in reasonable agreement with the Monte Carlo simulations. High-resolution STEM bright field imaging illustrates that the implanted Sb_2Te_3 surface layer is converted to an amorphous state from the ion beam-induced damage (Figure 1 f). The SRIM damage calculations indicate that the amorphous region occurs where the calculated displacement per atom (DPA)

exceeds an average of 1 DPA. Removing the crystal order is a known strategy to increase the bulk resistance of Sb_2Te_3 in phase-change devices; however, the topological surface states are generally believed to require a crystalline symmetry. Consequently, we explored methods to recrystallize the surface region using heat treatment methods.

As the melting point of Sb_2Te_3 is low (620 °C), there is a limited temperature window for high-temperature annealing. Heating was initially performed in-situ in a TEM on a hot-stage at increments of 50 °C apart, with an average ramp-rate of 10 °C / minute between the steps. Heating to a moderate temperature of 200 °C proved to be sufficient to observe the onset of recrystallization in the surface region. Figure 2 shows the sample after in-situ heating to a maximum of 250 °C and subsequent cooling. From STEM images, the fringes corresponding to the vdW gap between the Sb_2Te_3 quintuple layers are observable all of the way up to the surface. Away from the surface, higher-resolution imaging (Fig. 2 inset) shows the clear details of the quintuple layers (QLS) in Sb_2Te_3 layer, confirming the (001) direction is normal to the surface, and the images are taken with the electron beam parallel to the (120) projection in the hexagonal representation. Although crystallinity is restored in the region that was initially amorphous, there is evidence of localised disorder in the lattice planes which appear to include dislocations (e.g. the white white line).

Ex-situ heating was then performed on mm^2-sized specimens in a 1 atmosphere of nitrogen up to 250 ºC for 2 hours. The STEM image of the nitrogen-annealed Sb_2Te_3 is shown in Figure 3a, indicating crystallinity up to the TiO_2 interface. Unlike the in-situ heated STEM flake, discussed previously, the single crystal section appears to be free of dislocations and stacking faults. The atomic percentages of the local chromium concentration were extracted from EDS mapping overlayed in Figure 3b, showing that the peak Cr concentration (20 atomic %) straddles the Sb_2Te_3/TiO_2 interface for a thin region (~ 3 nm), whereas the doping concentration of Cr 5 nm below the interface is approximately 5 atom percent. Based on these results, it is possible that the Cr diffuses towards the interface during heating, and that the TiO_2 coating partially traps Cr. Near edge X-ray absorption fine structure (NEXAFS) spectroscopy at the Cr $L_{2,3}$ edges was performed at the Australian Synchrotron to analyse the valence state of the transition metal using surface-sensitive total electron yield (TEY) and bulk-sensitive fluorescence yield (FY) measurements. Cr signals were observed in TEY and FY modes for the heat-treated implanted TiO_2/Sb_2Te_3 and are plotted in Figure 3d, along with reference spectra for Cr oxide and chromium metal taken from Ref[24]. The presence of a multiplet of peaks at the Cr $L_{2,3}$ edges is an unambiguous indicator of high oxidation state, such as Cr^{3+}, because neutral transition metals present a single featureless peak[18]. The overall similarity of the TEY and FY signal suggests uniform doping up to a depth of tens of

nanometres comparable with the depth of Cr distribution. The absence of a detectable metal fraction of Cr in the Sb_2Te_3 is quite different from implantation studies in other dilute magnetic semiconductors which reported that frequently Co^0, Mn^0 and Cr^0 states are formed owing to ultra-small metallic clusters[25]. The presence of a high oxidation state suggests that the Cr acts as a substitutional dopant within the Sb_2Te_3 and TiO_2.

Additional insight into the local chromium state can be provided by magnetometry. $Cr_xSb_{2-x}Te_3$ is generally ferromagnetic, whereas both Cr_2O_3 and Cr_3O_4 are both antiferromagnetic and $Cr_{1-x}Ti_xO_2$ is generally paramagnetic. Vibrating sample magnetometry (VSM) measurements were performed on a Quantum Design Physical Property Measurement System (PPMS) for the unimplanted and heat-treated implanted crystals between 3 – 300 K. Figure 3c shows the strong diamagnetic signal for the unimplanted Sb_2Te_3 resulting in a negatively sloped, linear response characteristic of the bulk crystal. After implantation, a small positive non-linear signal from the implanted region becomes superimposed on the diamagnetic response. There is no observable coercive field within the instrument resolution (<10 Oe) at any temperature. However, there is an observable increase in the magnetic moment below 50 K. Measurements, both in-plane and out-of-plane, yielded similar results. As the diamagnetic response of Sb_2Te_3 is itself temperature-dependent, and a fraction of the Cr is in the TiO_2 layer, it is impossible to isolate the response of the Cr species purely in the Sb_2Te_3 region. However, by using the control measurement normalized by mass to subtract the Sb_2Te_3 diamagnetic susceptibility at the same temperature, and correcting for sample area, it is possible to estimate the total moment associated with each Cr dopant using the formula $< M > = \frac{CM_T}{FA}$ where M_T is the total moment after diamagnetic subtraction (in emu units), F is the ion fluence (in ions/ cm^2), A is the area and C is a constant of proportionality given as 9.274×10^{-21} μ_B emu^{-1}. Using this approach, the average moment approaches 1.5 μ_B per Cr ion (inset Fig 3 c). This is much higher than in antiferromagnetic CrO phases, however, it is slightly lower than the Hund's rule expectation value for a fully-ferromagnetic Cr^{3+} which would nominally give 3 μ_B in 3d3 configuration. Previous reports on similar pristine MBE-grown Cr-doped chalcogenide topological insulators generally show values between 1 - 2 μ_B per Cr ion and a similar low coercive field[26].

In conclusion, ion beam modification using Cr can achieve a range of functions in Sb_2Te_3 including forming amorphous layers and introducing high-temperature magnetic properties This demonstrates strong prospects for engineering topological insulators to achieve surface-dominated transport effects. It is anticipated that ion beam techniques can be applied to pattern topological insulator materials to locally adjust surface-state transport. It will be advantageous in the future to study thinner flakes to achieve

surface-dominated Anomalous Hall signals, and to explore the underlying physics of the magnetism using polarised neutron reflectometry and X-ray magnetic circular dichroism.

Figures – attached separately. Captions are below.

Figure 1. Schematic of the synthesis steps used in this work. a) Initially, a c-axis orientated Sb_2Te_3 crystal was cleaved to reveal a flat surface; b) The surface is coated using conformal atomic layer deposition of a TiO_2 oxide c) A low energy ion beam is used to implant the Cr through the oxide layer into the Sb_2Te_3 layer; d) Cross-sectional low-magnification HAADF image of the TiO_2/Sb_2Te_3 interface; e) Monte Carlo simulations predict that the majority of the chromium stops within 60 nm of the Sb_2Te_3 surface; f) EDS elemental mapping in the STEM cross-section shows that Cr –distribution is in reasonable agreement with the simulations; f) High-resolution STEM bright-field image reveals that, while the bulk of the Sb_2Te_3 (bottom) is crystalline, the implanted region (top) is amorphous.

Figure 2. Cross-sectional STEM HAADF after in-situ heat treatment to 200 °C showing that the amorphous region recrystallizes, however, crystalline defects are present. The inset shows High-resolution HAADF images of the quintuple layers which confirm the orientation of the crystal and reveal the van der Waals gap together with the crystal structure of the trigonal Sb_2Te_3 unit cell.

Figure 3. a) Cross-sectional HAADF image taken from a bulk sample after ex-situ heat treatment at 250 °C in a nitrogen atmosphere. Crystalline quintuple layers are evident up to the surface; b) EDS mapping of the cross-section and associated line profiles of the elements across the TiO_2/Sb_2Te_3 interface; c) Magnetic hysteresis measurements of the heat-treated Sb_2Te_3 substrate compared with the unimplanted sample. The inset shows a diamagnetic-corrected hysteresis loop at 5 K. d) NEXAFS spectroscopy at the Cr $L_{2,3}$ edges in total electron yield and fluorescence yield mode, revealing that the Cr^{3+} valence state is present in the implanted sample.

ACKNOWLEDGMENTS

DC acknowledges the support of the Australian Research Council (ARC) via DE180100314. DQ acknowledges the support of the Australian Research Council (Grant No. FT160100207). This work was partly supported by the ARC Centre for Excellence in Future Low Energy Electronics (CE170100039). This research used the JEOL JEM-ARM200F funded by the ARC LIEF grant (LE120100104). Ion beam implantation was performed using the facilities at the Centre for Accelerator Science, at the Australian Nuclear Science and Technology Organisation (P7437). Part of this research was undertaken on the Soft X-ray Spectroscopy beamline at the Australian Synchrotron, part of ANSTO. Research activities at the CAS including operation of the LEII / accelerator systems are funded by the NCRIS program by the Australian government.

DATA AVAILABILITY STATEMENT

The data that support the findings of this study are openly available in Zenodo at http://doi.org/ 10.5281/zenodo.3711602, reference number [27].

REFERENCES

[1]H. Zhang, C.-X. Liu, X.-L. Qi, X. Dai, Z. Fang, and S.-C. Zhang, Nat. Phys. **5**, 438 (2009).
[2]R. Yoshimi, A. Tsukazaki, K. Kikutake, J. G. Checkelsky, K. S. Takahashi, M. Kawasaki, and Y. Tokura, Nat. Mat. **13**, 253 (2014).
[3]M. Z. Hasan and C. L. Kane, Rev. Mod. Phys. **82** (4), 3045 (2010).
[4]X.-L. Qi and S.-C. Zhang, Rev. Mod. Phys. **83** (4), 1057 (2011).
[5]Y. L. Chen, J. G. Analytis, J. H. Chu, Z. K. Liu, S. K. Mo, X. L. Qi, H. J. Zhang, D. H. Lu, X. Dai, Z. Fang et al., Science **325** (5937), 178 (2009); K. Nakayama, S. Souma, C. X. Trang, D. Takane, C. Chen, J. Avila, T. Takahashi, S. Sasaki, K. Segawa, M. C. Asensio et al., Nano. Lett. **19** (6), 3737 (2019).
[6]Y. S. Hor, J. G. Checkelsky, D. Qu, N. P. Ong, and R. J. Cava, J. Phys. Chem. Sol. **72** (5), 572 (2011).
[7]J. Moon, N. Koirala, M. Salehi, W. Zhang, W. Wu, and S. Oh, Nano. Lett. **18** (2), 820 (2018).
[8]Y. Li, J. Zhang, G. Zheng, Y. Sun, S. S. Hong, F. Xiong, S. Wang, H. R. Lee, and Y. Cui, ACS Nano **9** (11), 10916 (2015).
[9]C.-Z. Chang, J. Zhang, X. Feng, J. Shen, Z. Zhang, M. Guo, K. Li, Y. Ou, P. Wei, L.-L. Wang et al., Science **340** (6129), 167 (2013).
[10]M. Wang, Y. Song, L. You, Z. Li, B. Gao, X. Xie, and M. Jiang, Sci. Rep. **6**, 22713 (2016).
[11]R. W. Hamm, *Industrial Accelerators and Their Applications*. (World Scientific, 2011), p.436.
[12]S. Pezzagna, B. Naydenov, F. Jelezko, J. Wrachtrup, and J. Meijer, New J. Phys. **12** (6), 065017 (2010); M. Schleberger and J. Kotakoski, Materials. **11**, 1885. (2018).
[13]V. Sacksteder, T. Ohtsuki, and K. Kobayashi, Phys. Rev. Appl. **3** (6), 064006 (2015).
[14]Z. Zhang, S. Song, Z. Song, Y. Cheng, Y. Gu, and B. Chen, Appl. Phys. Lett. **102** (25), 252106 (2013).
[15]P. A. Sharma, A. L. Lima Sharma, M. Hekmaty, K. Hattar, V. Stavila, R. Goeke, K. Erickson, D. L. Medlin, M. Brahlek, N. Koirala et al., Appl. Phys. Lett. **105** (24), 242106 (2014).
[16]W. A. MacFarlane, C. B. L. Tschense, T. Buck, K. H. Chow, D. L. Cortie, A. N. Hariwal, R. F. Kiefl, D. Koumoulis, C. D. P. Levy, I. McKenzie et al., Phys. Rev. B **90** (21), 214422 (2014).
[17]R. M. L. McFadden, A. Chatzichristos, K. H. Chow, D. L. Cortie, M. H. Dehn, D. Fujimoto, M. D. Hossain, H. Ji, V. L. Karner, R. F. Kiefl et al., Phys. Rev. B **99** (12), 125201 (2019).
[18]B. Leedahl, D. W. Boukhvalov, E. Z. Kurmaev, A. Kukharenko, I. S. Zhidkov, N. V. Gavrilov, S. O. Cholakh, P. H. Le, C. W. Luo, and A. Moewes, Sci. Rep. **7** (1), 5758 (2017).
[19]J. S. Dyck, Č. Drašar, P. Lošták, and C. Uher, Phys. Rev. B **71** (11), 115214 (2005).
[20]Z. Zhou, C. Uher, M. Zabcik, and P. Lostak, Appl. Phys. Lett. **88** (19), 192502 (2006).
[21]W. Zhao, D. Cortie, L. Chen, Z. Li, Z. Yue, and X. Wang, Phys. Rev. B **99** (16), 165133 (2019).
[22]I. G. Brown, Rev. Sci. Inst. **65** (10), 3061 (1994).
[23]J. F. Ziegler and J. M. Manoyan, Nucl. Phys. **35** (3), 215 (1988).
[24]F. Delmotte, J. Meyer-Ilse, F. Salmassi, R. Soufli, C. Burcklen, J. Rebellato, A. Jérome, I. Vickridge, E. Briand, and E. Gullikson, J. Appl. Phys. **124** (3), 035107 (2018).
[25]D. L. Cortie, Y. Khaydukov, T. Keller, D. J. Sprouster, J. S. Hughes, J. P. Sullivan, X. L. Wang, A. P. Le Brun, J. Bertinshaw, S. J. Callori et al., ACS Appl, Mat. Int. **9** (10), 8783 (2017).
[26]W. Liu, D. West, L. He, Y. Xu, J. Liu, K. Wang, Y. Wang, G. van der Laan, R. Zhang, S. Zhang et al., ACS Nano **9** (10), 10237 (2015).
[27]D. L. Cortie, 10.5281/zenodo.3711602 (2020).

Applied Physics Letters

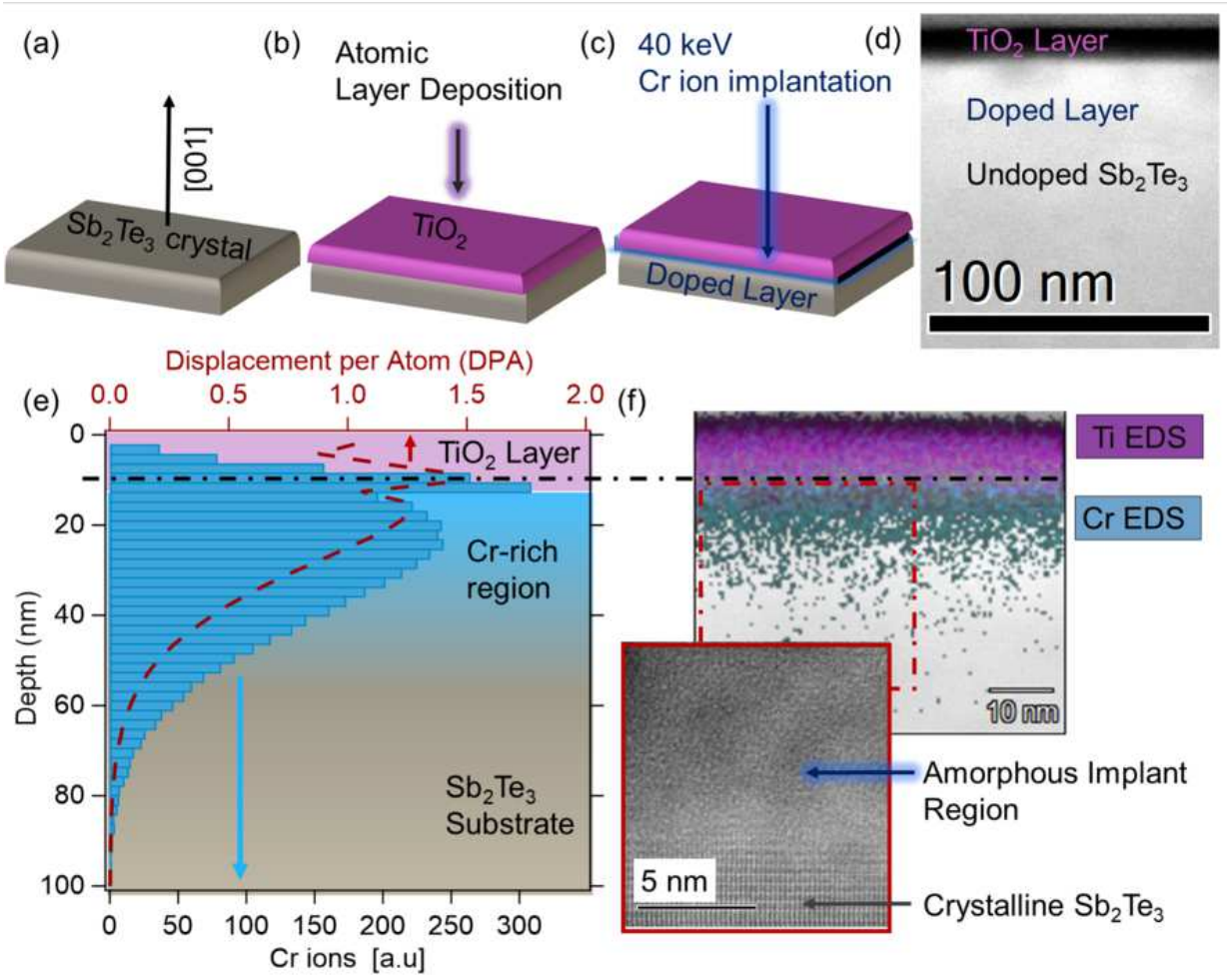

PLEASE CITE THIS ARTICLE AS DOI: 10.1063/5.0006447